A TWO-LAYER MODEL FOR THE LASER GENERATION OF ULTRASOUND IN GRAPHITE-EPOXY LAMINATES

M. Dubois, F. Enguehard, L. Bertrand
École Polytechnique de Montréal, Département de Génie Physique
C.P. 6079, succ. Centre-Ville
Montréal, Québec, Canada H3C 3A7

INTRODUCTION - WHY A TWO-LAYER MODEL ?

We previously reported the performances of a numerical simulation model [1] that calculates the mechanical displacements induced within a sample by the absorption of a laser pulse. This model solves the heat diffusion and acoustic wave propagation equations over an orthotropic slab of finite thickness with the help of temporal Laplace and spatial 2D Fourier transformations. The parallel and normal displacements predicted by the model were found to be in generally very good agreement with experimental data obtained on various samples in various excitation conditions. Among these experiments, one consisted in the CO_2 laser excitation of a graphite-epoxy sample. We performed an optical study of the graphite-epoxy composite using FTIR photoacoustic spectroscopy [2] to determine the optical penetration depth spectrum of this material. This study revealed that a thin ($\approx$ 30 μm thick) epoxy layer covered the top graphite fiber sheet of the composite, and that the optical penetration depth of the CO_2 radiation in the epoxy was about 20 μm. Consequently, when a CO_2 laser pulse impinges on the composite, all the radiation is absorbed in the epoxy layer, and it is easy to simulate this situation with the model, using the rigidity-expansion tensor [λ] of the epoxy for the generation and the rigidity tensor [C] of the composite for the propagation (see [1]).

On the other hand, the mechanism of generation is completely different when the composite is excited by a Nd:YAG laser pulse. The epoxy is completely transparent to the YAG wavelength, so that the radiation travels through the epoxy layer and reaches the top graphite fiber sheet where it is immediately absorbed. Our current one-layer model cannot simulate these conditions of generation, in which the thermal expansion sources (i.e. the graphite fibers having absorbed the radiation) are constrained by the epoxy layer; an evolution of the model is required.

The effects of a constraining layer on the features of the laser generated acoustic waves have already been studied experimentally by many authors [3-7]. The most noticeable one is a much greater production of longitudinal waves propagating along the normal to the irradiated surface. This feature has been exploited by Carome [8] and Felix [9] to increase the signal-to-noise ratios of their experiments. Some authors have proposed two- or multi-layer models to analyze the constraining layer configuration

Review of Progress in Quantitative Nondestructive Evaluation, Vol. 14
Edited by D.O. Thompson and D.E. Chimenti, Plenum Press, New York, 1995

[3,4,10-12]. Unfortunately, all these models being 1D, they are limited to uniform irradiations. Therefore, a more general two-layer 3D model is needed to observe the "non-1D" phenomena induced by the presence of a constraining layer.

PRESENTATION OF THE TWO-LAYER MODEL

We have extended the field of application of the one-layer model to two-layer geometries. The sample is now composed of two infinite slabs S_1 and S_2, of finite thicknesses L_1 and L_2, made of two orthotropic materials having their own optical, thermal, thermo-mechanical and mechanical properties. As in the one-layer model, it is assumed that each slab is cut in such a way that the normal to its surfaces corresponds to one of its principal axes. Furthermore, the relative orientation of the slabs is supposed to be such that their principal axes parallel to the surfaces merge. An important assumption of the two-layer model, that was not made in the one-layer one, is the neglection of the thermal conduction within the slabs. This assumption is acceptable in the two-layer model because this model is going to simulate constrained thermoelastic sources which generate much greater precursors than the thermal conduction induced ones [6]. The temperature elevation fields $\vartheta_1(x,y,z,t)$ in S_1 and $\vartheta_2(x,y,z,t)$ in S_2 are then dictated by the optical absorption only, and, the laser beam entering the sample through the surface of S_1 and being completely transmitted at the interface between S_1 and S_2 without any reflection (the possibility of creation of a stationary electromagnetic wave induced thermoelastic source grating is not envisaged here), their mathematical expressions are:

$$\text{in } S_i \ (i = 1,2) \qquad \vartheta_i(x,y,z,t) = \frac{\beta_i E}{\rho_i C_{pi}} g(x,y)\, e^{(\beta_i - \beta_1)L_1 - \beta_i z} \int_0^t f(\tau)d\tau \qquad (1)$$

In these two formula, the z axis is normal to the surfaces of the slabs, and the x and y axes are parallel to these surfaces. The indices 1 and 2 refer to the physical properties of the slabs S_1 and S_2: the β_i are the optical absorption coefficients at the excitation wavelength, the ρ_i the densities, and the C_{pi} the specific heats. E is the portion of the laser pulse energy E_{pulse} that really "enters" the two-layer sample, i.e. $E = (1-R_1)\, E_{pulse}$, R_1 being the reflection coefficient at the excitation wavelength of the irradiated surface of S_1. Finally, g(x,y) and f(t) are the normalized surface and time profiles of the laser radiation.

The mechanical displacement fields $\vec{u}_1(x,y,z,t)$ in S_1 and $\vec{u}_2(x,y,z,t)$ in S_2 are dictated by the acoustic wave propagation equations with thermal expansion sources, which are, using Auld's abbreviated notation [13]:

$$\text{in } S_i \ (i = 1,2) \qquad \rho_i \frac{\partial^2 \vec{u}_i}{\partial t^2} = \nabla.\left([C_i] : \nabla_s \vec{u}_i\right) - [\lambda_i].\nabla\vartheta_i \qquad (2)$$

where the $[C_i]$ are the rigidity tensors and the $[\lambda_i]$ the rigidity-expansion tensors given by $[\lambda_i] = [C_i]:[\alpha_i]$, the $[\alpha_i]$ being the thermal expansion tensors.

These two propagation equations come with initial and boundary conditions. As in the one-layer model, both displacements and speeds are assumed to be zero at $t = 0$, and the two surfaces of the sample, of equations $z = 0$ and $z = L_1+L_2$, are supposed to be mechanically unconstrained. As regards the boundary conditions at the interface between the slabs, the mechanical contact between them is assumed to be perfect, so that both displacements and stresses are conserved. Hence, the initial and boundary conditions are:

$$\text{at } t = 0 \qquad \vec{u}_1 = \vec{u}_2 = \vec{0} \text{ and } \frac{\partial \vec{u}_1}{\partial t} = \frac{\partial \vec{u}_2}{\partial t} = \vec{0} \tag{3}$$

$$\text{at } z = 0 \ (i = 1) \text{ and at } z = L_1 + L_2 \ (i = 2) \qquad [\sigma_i].\vec{z} = \vec{0} \tag{4}$$

$$\text{at } z = L_1 \qquad \vec{u}_1 = \vec{u}_2 \text{ and } [\sigma_1].\vec{z} = [\sigma_2].\vec{z} \tag{5}$$

As in the one-layer model, the set of equations (2,3,4,5) is solved analytically in the Laplace and 2D Fourier spaces, and the only numerical step consists in performing numerical inverse Laplace and 2D Fourier transformations to obtain the displacement fields in the "real" spaces. No particular assumptions about the surface and time profiles g(x,y) and f(t) of the laser radiation are needed for the resolution, so that the model can solve the displacement fields for any conditions of irradiation.

CONFRONTATION OF THE TWO-LAYER MODEL TO EXPERIMENTAL DATA

All the experiments that will be presented were performed with a Nd:YAG source for the generation and an optical probe for the detection. The YAG source is a pulsed monomode laser, with a pulse energy adjustable between 1 and 100 mJ, a pulse duration variable between 10 and 90 ns (depending on the pulse energy), a Gaussian radius at 1/e of the beam of 1.4 mm, and a repetition rate adjustable between 0.1 and 50 Hz. The optical probe is a *Ultra-Optec OP-35-I/O* optical heterodyne interferometer, that can measure both parallel and normal displacements to the surface [14]. The detection limit of this interferometer is a few Å, and its bandpass spreads from 1 kHz to 35 MHz.

Confrontation of the Model to a First Experimental Result

The first sample that we made consisted in a 1.0 mm thick glass plate stuck over a 4.7 mm thick aluminum plate with an epoxy glue. Its glass side was impinged on by a Nd:YAG laser radiation 7.8 mJ in energy and 12 ns in pulse duration. Prior to excitation, the Gaussian beam was sent through a circular aperture 2.0 mm in diameter. We reproduced this experiment with the two-layer model, giving S_1 the physical properties of the glass and S_2 those of the aluminum. The optical, thermal and thermo-mechanical properties were taken from the literature, but the rigidity tensors were measured with piezoelectric transducers. The irradiation was supposed to be uniform over a disk 2.0 mm in diameter, and E was taken to be 7.8 mJ.

Figure 1 confronts the calculated and experimental normal displacement curves at the epicenter on the opposite side to the excitation. We had to multiply the calculated curve by a factor of 12% in order to make the two curves superimpose, which can be interpreted as follows. Concerning the optical phenomena, the only restriction of the model is the condition of zero reflection at the interface between S_1 and S_2, which means that, E being the energy "entering" S_1, $E \exp(-\beta_1 L_1)$ is the energy "going out of" S_1 and "entering" S_2, and $E \exp(-\beta_1 L_1 - \beta_2 L_2)$ is the energy "going out of" S_2. In the case of a two-layer sample made of a completely transparent slab and of a highly absorbing one ($\beta_i L_i << 1$ and $\beta_j L_j >> 1$, with (i,j) = (1,2) or (2,1)), E appears to be the energy absorbed by the absorbing slab. In the simulation we took for E the value of the laser pulse energy; the superimposition of the curves in figure 1 revealed that only 12% of this incident energy was absorbed at the surface of the aluminum, which is a reasonable value.

The two first acoustic pulses (at 0.7 μs and 1.1 μs) of the experiment are quite well reproduced by the model. On the other hand, for times larger than 1.2 μs, the two

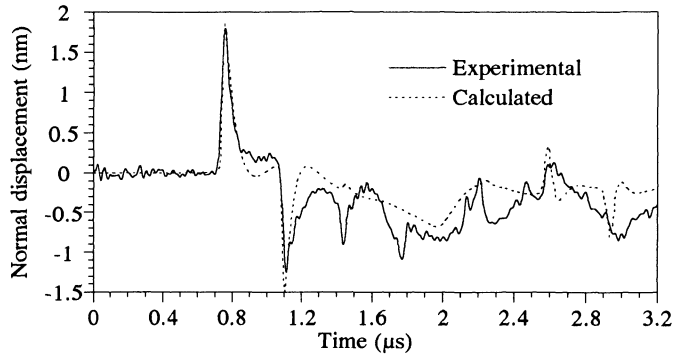

Figure 1. Calculated and experimental normal displacement curves at the epicenter on the opposite side to the excitation. The sample is a glass-aluminum plate, and its glass side is impinged on by a Nd:YAG laser radiation.

curves do not superimpose any more. Moreover, the experiment shows acoustic pulses that are either not calculated (for example at 1.8 μs) or inversed (for example at 1.4 μs) by the simulation. These discrepancies are due to the presence of the thin (≈ 100 μm thick) epoxy glue layer separating the glass and the aluminum plates: our sample, in the experiment, behaves like a three-layer system. In the model, the acoustic impedances of the glass and the aluminum being very close to each other, the glass-aluminum interface produces very weak reflections of longitudinal waves. This is not the case in the experiment, because the epoxy glue has an acoustic impedance that is much smaller than those of the glass and the aluminum. This explains why certain acoustic pulses appearing in the experiment vanish in the simulation. The inversion of the polarizations of certain other experimental acoustic pulses in the simulation confirms the intrusive nature of the epoxy glue layer for our model; a "really two-layer" sample is necessary to check the validity of our work.

Improvement of the Sample - Validation of the Two-Layer Model

For the second sample that we made, the 4.7 mm thick aluminum plate was replaced by a 3.0 mm thick PVC one. The acoustic impedance of the PVC being very close to the one of the epoxy glue, this sample could reasonably be expected to have a real two-layer behavior. Its glass side was impinged on by a Nd:YAG laser radiation 9.7 mJ in energy, 16 ns in pulse duration, and 1.4 mm in Gaussian radius. For the simulation, we measured the rigidity tensor of the PVC with piezoelectric transducers. The absorption coefficient of the PVC at the YAG wavelength was also evaluated experimentally from the full width at half maximum of the acoustic pulse generated by a uniform irradiation (see [15]): we found a value of 10^4 m^{-1}. The other physical properties of the PVC were obtained from the manufacturer.

Figure 2 confronts the calculated and experimental normal displacement curves at the epicenter on the opposite side to the excitation. An absorption of 25% by the PVC plate was determined for the two curves to superimpose. The surface finish of the PVC plate being quite smooth, this value is acceptable. This time, the general agreement between the experiment and the simulation is good. The model reproduces all the acoustic pulses experimentally observed, with polarizations corresponding to the experimental

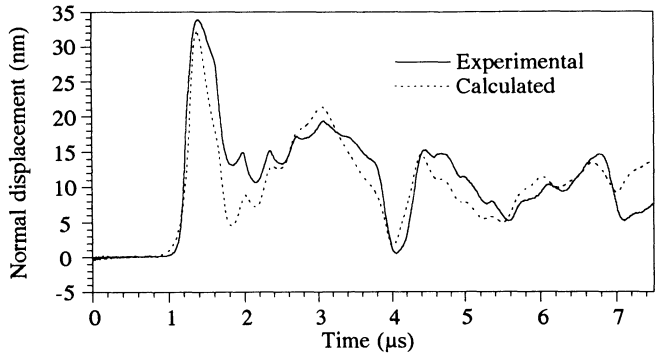

Figure 2. Calculated and experimental normal displacement curves at the epicenter on the opposite side to the excitation. The sample is a glass-PVC plate, and its glass side is impinged on by a Nd:YAG laser radiation.

ones. The discrepancies in the amplitudes and widths of the pulses between the experiment and the simulation can be attributed to a visco-elastic behavior of the PVC.

The two large pulses, visible at 1.3 μs and 4.0 μs, are produced by the longitudinal waves polarized along the z axis and created in the PVC by the thermoelastic effect. These waves are intense due to the important penetration of the YAG radiation in the PVC [16]. Moreover, the acoustic impedance of the glass being large as compared to the one of the PVC, the wave propagating in the $-\vec{z}$ direction towards the glass is primarily reflected at the interface and its polarization is inversed, so that the reflected wave propagating in the $+\vec{z}$ direction towards the free surface of the PVC has its polarization in phase with the one of the wave created in the PVC by the thermoelastic effect and propagating in the $+\vec{z}$ direction. This constructive superposition leads to the huge precursor at 1.3 μs. The large pulse at 4.0 μs is attributed to a return trip within the PVC plate of the longitudinal waves responsible for the precursor. The polarization of this pulse is inverse to the one of the precursor, once again in agreement with the relative values of the acoustic impedances of the glass and the PVC. The small pulses appearing between and after the two large pulses are due to multiple return trips within the glass plate of longitudinal waves having been transmitted from the PVC at the interface. The delay between two successive of these pulses confirms this interpretation. No shear wave effect is visible in figure 2. The constrained thermoelastic generation phenomenon accounts for that, as will be seen in the next section.

Confrontation of the Model to an Experimental Result in a Situation of Unconstrained Thermoelastic Generation

The glass-PVC sample of the last section was taken upside down and its PVC side was impinged on by a Nd:YAG laser radiation 13.8 mJ in energy, 16 ns in pulse duration, and 1.4 mm in Gaussian radius. In this configuration, the thermal expansion sources were not buried under a constraining layer any more.

Figure 3 displays the calculated and experimental normal displacement curves at the epicenter on the opposite side to the excitation. An absorption of 30% by the PVC plate was determined for the two curves to superimpose. This value is quite consistent with the one of 25% that we determined in the last section: this time, there are no optical

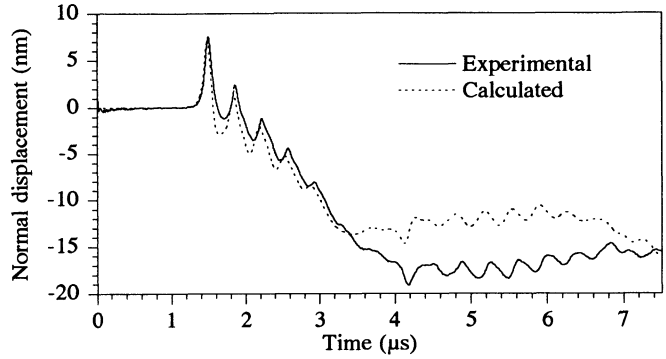

Figure 3. Calculated and experimental normal displacement curves at the epicenter on the opposite side to the excitation. The sample is a PVC-glass plate, and its PVC side is impinged on by a Nd:YAG laser radiation.

losses at the free surface or within the bulk of the glass. Here again, the model reproduces very faithfully all the acoustic pulses observed in the experimental curve. On the other hand, for times larger than 3.4 μs, the calculated and experimental curves do not superimpose any more: these two portions of the curves seem to be simply shifted from each other in the direction of the normal displacement. The appearance of this shift at 3.4 μs corresponds to the arrival on the free surface of the glass of the shear wave created in the PVC by the thermoelastic effect and having propagated in the $+\vec{z}$ direction. This shear wave is much more visible in the simulation than in the experiment, which can reasonably be explained by the fact that, if the model assumes a perfect mechanical contact between the two slabs, most probably it is not the case in the experimental field. One can easily understand that, whatever the quality of the adherence between the two slabs, the interface will efficiently transmit the normal stresses and displacements. On the other hand, the fulfillment of the condition of transmission of the parallel stresses and displacements by the interface demands a top quality mechanical contact between the two slabs. The discrepancy between the calculated and experimental displacements induced by the shear wave appears to be an indirect measurement of the quality of the adherence between the glass and PVC plates.

Simulation of the Nd:YAG Laser Thermoelastic Generation of Ultrasound in a Graphite-Epoxy Composite Sample with the Two-Layer Model

A last experiment was performed with a graphite-epoxy composite sample and a Nd:YAG irradiation. As seen earlier, the composite, when excited by this wavelength, behaves like a two-layer system, the first one being a thin ($\approx$ 30 μm thick) layer of epoxy, completely transparent to the radiation, and the second one being the bulk composite, highly absorbing the radiation. The 2.0 mm thick sample was impinged on by a YAG laser radiation 10.6 mJ in energy, 16 ns in pulse duration, and 1.4 mm in Gaussian radius. An about 100 nm thick aluminum layer was deposited by evaporation on the opposite side of the sample to the excitation in order to increase the signal-to-noise ratio of the detection. The simulation of the experiment required the knowledge of the physical properties of the materials constituting the two layers. The optical penetration depth of the YAG radiation in the epoxy was checked to be very large ($\approx$ 10 mm) as compared to the thickness of the epoxy layer. The thermal and thermo-mechanical properties of the epoxy were drawn from the literature [17], and its rigidity tensor was measured with piezoelectric

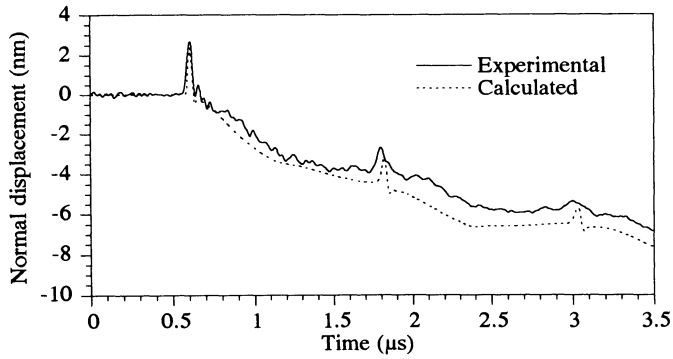

Figure 4. Calculated and experimental normal displacement curves at the epicenter on the opposite side to the excitation. The sample is a graphite-epoxy plate, and is impinged on by a Nd:YAG laser radiation.

transducers. Concerning the composite, the generation and the propagation occuring at different volume scales, we accounted for this point in the simulation. The YAG radiation being completely absorbed at the first graphite fiber sheet that it reaches, the optical penetration depth of the YAG radiation in the composite was chosen arbitrarily to be 1 μm (simulations with values of 0.1 μm, 1 μm and 8 μm yielded exactly the same results), and its rigidity-expansion tensor was evaluated with the mechanical and thermo-mechanical properties of a unidirectional graphite-epoxy composite (the corresponding tensors were found in [18]). On the other hand, the nine components of the rigidity tensor representative of the propagation were evaluated using a "cut pieces" technique [19]. Finally, the thermal properties of the composite were drawn from the literature [17].

Figure 4 compares the calculated and experimental normal displacement curves at the epicenter on the opposite side to the excitation. The calculation was performed with an absorption of 15% by the bulk composite and a Gaussian radius of the laser beam of 2.0 mm. With these values, the model reproduces the experiment quite accurately. The three acoustic pulses, visible at 0.6 μs, 1.8 μs and 3.0 μs, are produced by the longitudinal wave generated under the epoxy layer and its successive echoes. Weak shear wave effects are also discernible at 1.2 μs and 2.4 μs, the latter time corresponding to waves having propagated through the sample twice as longitudinal and once as shear. Finally, the effects of dispersion and attenuation induced by the inhomogeneous nature of the composite appear clearly on figure 4: the third acoustic pulse, at 3.0 μs, is much broader in time and much weaker in amplitude in the experiment than in the simulation.

The Gaussian radius of the irradiation had to be increased in the model for the calculated curve to fit to the experimental one. This can perhaps be justified by an axial thermal conduction effect within the graphite fibers that have absorbed the radiation or by an optical diffusion effect within the epoxy layer, both effects inducing a broadening of the thermoelastic source.

Only 15% of the incident energy was used to launch acoustic waves in the composite. This weak efficiency can be due to the complexity of the thermoelastic generation process in this material. The optical energy is absorbed by the graphite fibers, but these fibers have small thermal expansion coefficients and are weak thermoelastic sources. On the other hand, the epoxy surrounding these fibers exhibits a high thermal

expansion coefficient and constitutes the actual thermoelastic source of the composite. But the heat must flow from the graphite fibers to the surrounding epoxy; thermal resistance effects between the fibers and the epoxy can explain the weak conversion of thermal energy to mechanical energy in the composite.

CONCLUSION

Our new model has been shown to be able to simulate the thermoelastic generation of ultrasound in two-layer samples. Apart from the common applications with the one-layer model (study of the generation, propagation, dispersion and attenuation of ultrasound), this model will also be used specifically for the mechanical qualification of interfaces.

REFERENCES

1. M. Dubois, F. Enguehard, M. Choquet, J.-P. Monchalin and L. Bertrand, in *Review of Progress in QNDE*, Vol. 13, eds. D. O. Thompson and D. E. Chimenti (Plenum, New York, 1994), p. 1023.
2. M. Dubois, F. Enguehard, M. Choquet, J.-P. Monchalin and L. Bertrand, in *Review of Progress in QNDE*, Vol. 13, eds. D. O. Thompson and D. E. Chimenti (Plenum, New York, 1994), p. 441.
3. L. S. Gournay, J. Acoust. Soc. Am. 40 (6), 1322 (1966).
4. J. C. Bushnell and D. J. McCloskey, J. Appl. Phys. 39 (12), 5541 (1968).
5. R. J. Von Gutfeld and R. L. Merlcher, Appl. Phys. Lett. 30 (6), 257 (1977).
6. R. J. Dewhurst, D. A. Hutchins, S. B. Palmer and C. B. Scruby, J. Appl. Phys. 53 (6), 4064 (1982).
7. D. A. Hutchins, R. J. Dewhurst and S. B. Palmer, Ultrasonics 19 (3), 103 (1981).
8. E. F. Carome, N. A. Clark and C. E. Moeller, Appl. Phys. Lett. 4 (6), 95 (1964).
9. M. P. Felix, Rev. Sci. Instrum. 45 (9), 1106 (1974).
10. G. C. Wetsel, IEEE Transactions UFFC 33 (5), 450 (1986).
11. C. Thomsen, H. T. Grahn, H. J. Marris and J. Tauc, Phys. Rev. B 34 (6), 4129 (1986).
12. Z. Bozoki, A. Miklos, C. Glorieux, J. Thoen and D. Bicanic, Journal de Physique (1994), to be published.
13. B. A. Auld, *Acoustic Fields and Waves in Solids*, Vol. 1, R. E. Krieger Publishing Company (Malabar, Florida, 1990).
14. J.-P. Monchalin, J.-D. Aussel, R. Héon, C. K. Jen, A. Boudreault and R. Bernier, J. Nondestruct. Eval. 8 (2), 121 (1989).
15. M. Dubois, F. Enguehard and L. Bertrand, Phys. Rev. E 50 (2) (1994), to be published.
16. M. Dubois, F. Enguehard, M. Choquet, J.-P. Monchalin and L. Bertrand, Journal de Physique (1994), to be published.
17. *Engineering Materials Handbook*, Vol. 1: *Composites*, and *Engineering Materials Handbook*, Vol. 2: *Engineering Plastics*, ASM International (USA, 1988).
18. C. Corbel, F. Guillois, D. Royer, M. Fink and R. De Mol, IEEE Transactions UFFC 40 (6), 710 (1993).
19. R. D. Kriz and W. W. Stinchcomb, Exp. Mech. 19, 41 (1979).